ATP Binding Properties of the Soluble Part of the KdpC Subunit from the *Escherichia coli* K^+-Transporting KdpFABC P-Type ATPase†

Franziska Ahnert, Roland Schmid, Karlheinz Altendorf, and Jörg-Christian Greie*

Universität Osnabrück, Fachbereich Biologie/Chemie, Abteilung Mikrobiologie, D-49069 Osnabrück, Germany

Received June 19, 2006; Revised Manuscript Received July 26, 2006

ABSTRACT: P-Type ATPases catalyze the transport of cations across the cell envelope via site-specific hydrolysis of ATP. Modulation of enzyme activity by additional small subunits and/or a second regulatory nucleotide binding site is still a subject of discussion. In the K^+-transporting KdpFABC complex of *Escherichia coli*, KdpB resembles the catalytic P-type ATPase subunit, but ATP binding also occurs in the essential but noncatalytic subunit, KdpC. For further characterization, the soluble portion of KdpC ($KdpC_{sol}$, residues Asn39−Glu190) was synthesized separately and purified to homogeneity via affinity and size exclusion chromatography. Protein integrity was confirmed by N-terminal sequencing, mass spectrometry, and circular dichroism spectroscopy, which revealed an α-helical content of 44% together with an 8% β-sheet conformation consistent with the values deduced from the primary sequence. The overall protein structure was not affected by the addition of ATP to a concentration of up to 2 mM. In contrast, labeling of $KdpC_{sol}$ with the photoreactive ATP analogue 8-azido-ATP resulted in the specific incorporation of one molecule of 8-azido-ATP per peptide. No labeling could be observed upon denaturation of the protein with 0.2% sodium dodecyl sulfate, which suggests the presence of a structured nucleotide binding site. Labeling could be inhibited by preincubation with either ATP, ADP, AMP, GTP, or CTP, thus demonstrating a low specificity for nucleotides. Following 8-azido-ATP labeling and tryptic digestion of $KdpC_{sol}$, mass spectrometry showed that ATP binding occurred within the Val144−Lys161 peptide located within the C-terminal part of KdpC, thereby further demonstrating a defined nucleotide binding site. On the basis of these findings, a cooperative model in which the soluble part of KdpC activates catalysis of KdpB is suggested.

P-Type ATPases are ubiquitously abundant primary ion pumps, which are capable of transporting cations across the cell membrane at the expense of ATP (*1*). These ions comprise a large variety of biochemical functions, for example, enzyme cofactors and cosubstrates for sym- and antiport, and they are involved in the maintenance of cytoplasmic pH and turgor. Thus, nature has developed rather sophisticated transport machineries that ensure substrate supply even against large concentration gradients. Due to the importance of these enzymes, representatives of eukaryotic P-type ATPases and especially the sarcoplasmic reticulum Ca^{2+}-ATPase have been studied intensively, resulting in detailed structural and functional information about their mode of action (*2*−*4*). During catalysis, P-type ATPases cycle between the so-called E1 and E2 states, each of which comprises different structural properties together with different binding affinities for both ATP and the transport substrate. Crucial for catalysis is the reversible phosphorylation of a conserved aspartate (*1*), which is the main trigger for the conformational changes within the protein.

In contrast to these well-studied and closely related eukaryotic P-type ATPases, much less is known about their homologues in bacteria. Whereas in eucarya there is predominantly only one subunit, which builds up the transport system, in bacteria there are multiple polypeptides involved in the formation of the active enzyme. Such a rather unusal prokaryotic P-type ATPase is the KdpFABC complex of the enterobacterium *Escherichia coli*. This complex serves as a highly specific K^+ transporter, which is only synthesized in case of K^+ limitation when the cell's constitutive K^+ transport systems can no longer supply the cell with K^+ (*5*). An absolutely unique feature of this member of the P-type ATPase group is that catalytic activity (i.e., ATP hydrolysis) and substrate transport (i.e., K^+ translocation) occur on two different polypeptides, namely, KdpB and KdpA, respectively (*6*). Whereas KdpB (72 kDa) comprises all features characteristic of P-type ATPases, KdpA (59 kDa) is homologous to K^+ channels of the KcsA type (*6*, *7*). For communication between the sites of ATP hydrolysis and ion transport, two conserved charged residues within a transmembrane helix of KpdB where shown to be essential (*8*). Much less is known about the smaller subunits KdpF (3 kDa) and KdpC (20 kDa). Whereas the former has been shown to stabilize the transport complex in vitro (*9*), the latter is reported to be an essential part of the transport complex (*10*). On the basis of sequence analysis, KdpC is supposed to contain just

† Supported by the Deutsche Forschungsgemeinschaft (SFB 431) and by the Fonds der Chemischen Industrie.

* To whom correspondence should be addressed: Universität Osnabrück, Fachbereich Biologie/Chemie, Abteilung Mikrobiologie, D-49069 Osnabrück, Germany. Telephone: +49-541-9692809. Fax: +49-541-9692870. E-mail: greie@biologie.uni-osnabrueck.de.

10.1021/bi061213p CCC: $33.50
Published on Web 08/18/2006

one transmembrane helix in the N-terminal region with the rest of the polypeptide facing the cytoplasm. Together with secondary structure prediction, hydropathy plot analysis, and extensive sequence alignments, the polypeptide comprises four domains, two of which are highly conserved among different organisms and located within the hydrophilic portion of KdpC (*10*). Although this stretch of residues is the only larger hydrophilic domain of the KdpFABC complex beside the B, N, and A domains of the catalytic KdpB subunit, its function is still unknown. An orthologous stabilizing role has been discussed with respect to the β-subunit of Na^+,K^+- and H^+,K^+-ATPase (*11*). However, since the soluble extension of the β-subunit faces the extracellular space, a corresponding function of KdpC seems unlikely due to an opposing inward orientation of the hydrophilic part. On the other hand, several small proteins exist within the P-type ATPase superfamily like phospholamban or calmodulin in the case of the Ca^{2+}-ATPase (*12*) or the γ-subunit in case of Na^+,K^+-ATPase (*13*), which exert a regulatory function on enzyme activity via interactions with the large cytoplasmic loop of the pump. *Neurospora crassa* H^+-ATPase, which is also a single-subunit P-type ATPase, contains an intrinsic hydrophilic regulatory R domain at the C-terminus, which is proposed to interact with the catalytic N and P domains (*14*). Thus, modulation of P-type ATPase activity or ATP affinity by small polypeptides comprising just one transmembrane span together with a hydrophilic extension, which interacts with the catalytic domains of the pump, is likely to be a common principle.

It has been demonstrated that when the KdpFABC complex is labeled with the photoreactive ATP analogue 2-azido-ATP, in addition to KdpB KdpC was labeled significantly (S. Dröse and K. Altendorf, unpublished results). This argues in favor of a regulatory function of KdpC either via interaction with the nucleotide binding pocket of KdpB or via ATP binding itself. To further substantiate this view, we expressed and purified the hydrophilic portion of the polypeptide ($KdpC_{sol}$) corresponding to residues Asn39−Glu190. The purified protein was analyzed with respect to its biochemical characteristics, structural composition, and ATP binding properties. $KdpC_{sol}$ was shown to specifically bind one molecule of ATP per polypeptide but with rather low nucleotide specificity. The site of ATP binding could be located between residues Val144 and Lys161 near the C-terminus of the polypeptide and most likely close to the nucleotide binding domain of KdpB within the assembled enzyme complex. These findings support the idea that enzyme activity or ATP affinity in P-type ATPases is modulated by interactions of hydrophilic portions of the enzyme with the catalytic domain.

EXPERIMENTAL PROCEDURES

Bacterial Strains and Growth Conditions. E. coli strain BL21 (Novagen) was transformed with plasmid pET-kdpCsol and grown on LB-rich medium (*15*) supplemented with carbenicillin (50 μg/mL) at 37 °C until an optical density (578 nm) of 0.7 was reached. Protein synthesis was induced by the addition of 1 mM IPTG,[1] and growth was allowed to proceed until an optical density of ~2.0 was reached. Cells were harvested by centrifugation (10000*g* for 10 min), frozen in liquid nitrogen, and stored at −80 °C.

Construction of Plasmids. The methods used for handling of recombinant DNA and for transformation of *E. coli* cells were as described previously (*15*). All sequence modifications were checked by sequencing. Plasmid pET-kdpCsol comprises a pET-16b (Novagen) vector background together with a *kdpC* insert, which was derived via PCR from plasmid pGS4, which is, in turn, a pSM5 derivative carrying the *kdpFABC* operon (*6*). With respect to pSM5, pGS4 comprises 14 additional histidine codons [$(CATCAC)_7$] at the 3′ end of the *kdpA* gene, which have been introduced into pSM5 via a standard two-step PCR technique by use of mutant primers and *Sac*II and *Bst*BI restriction sites flanking the 377 bp fragment of interest. Plasmid pGS4 was used as a template to amplify the 3′ part of the *kdpC* gene, which was then cloned into pET-16b as follows. The sequence of *kdpC* encoding C-terminal residues Asn39−Glu190 was amplified via a standard PCR technique by use of primers 5′-TCGTCATATG*AATGGTTCGTTGATTCGTGAA*-3′ (forward) and 5′-AGCCGGATCC*GTTATTCATCAAGTTTATCCAG*-3′ (reverse), with *Nde*I and *Bam*HI restriction sites underlined and KdpC-coding sequences italicized. The resulting PCR product was then cleaved with *Nde*I and *Bam*HI, and the resulting 466 bp fragment was ligated into the *Nde*I−*Bam*HI-digested pET-16b vector, which finally resulted in plasmid pET-kdpCsol.

Purification of $KdpC_{sol}$. Frozen cells were thawed and homogenized to 1 g/mL in 50 mM sodium phosphate (pH 7.4) and 0.5 mM PMSF. Cells were disrupted by sonication at 0 °C in six intervals of 1 min each by use of a Branson B15 cell disruptor at an output level of 6 with 50% pulsed. Cell debris were removed by low-speed centrifugation (20 min at 15000*g*), followed by a high-speed centrifugation (1.5 h at 180000*g*) to remove the membrane fraction. The supernatant was then provided with 100 mM NaCl and 10 mM imidazole and taken directly for affinity chromatography. The affinity resin (Ni-Sepharose 6 Fast Flow, Amersham Biosciences; 1 mL of slurry/10 mL of supernatant) was pre-equilibrated with 50 mM sodium phosphate (pH 7.4), 0.5 mM PMSF, 100 mM NaCl, and 10 mM imidazole and incubated with the supernatant for 1 h on ice with gentle shaking. The resin was then added to a glass column until it was and the column connected to an Äkta FPLC system (Amersham Biosciences) at a flow rate of 1 mL/min. Unbound protein was removed by washing with buffer. Unspecifically bound proteins were removed by increasing the imidazole concentration to 55 mM, whereas $KdpC_{sol}$ was subsequently eluted with 170 mM imidazole. Protein-containing fractions were pooled and concentrated approximately 25-fold using Amicon Ultra-4 Ultracell 5k centrifugal filter devices (Millipore) at 3000*g*. Proteolytic cleavage of the polyhistidine tag and removal of the factor Xa protease were carried out by using the Factor Xa Cleavage Capture Kit as recommended by the supplier (Novagen), with 50 mM sodium phosphate (pH 7.4) instead of the supplied factor Xa cleavage buffer, and the digestion was performed at 30 °C for 4 h. The cleaved affinity tag as well as residual uncleaved protein was subsequently removed by passage of

[1] Abbreviations: CD, circular dichroism; ESI-MS, electrospray injection mass spectrometry; ICD, ligand-induced circular dichroism; IPTG, isopropyl β-D-thiogalactopyranoside; MS, mass spectrometry; PMSF, phenylmethanesulfonyl fluoride; SDS, sodium dodecyl sulfate; TFA, trifluoroacetic acid.

the sample through 1 mL spin filters (10 s at 500*g*) filled again with pre-equilibrated Ni-Sepharose. For size exclusion chromatography, the sample was loaded on a 10/30 Superdex-75 gel filtration column (Amersham Biosciences), which was run at 0.5 mL/min in 50 mM sodium phosphate (pH 7.4) and 0.5 mM PMSF. Protein-containing fractions were pooled and concentrated as described above. Size calibration of the gel filtration column was conducted with a mixture of standard proteins (aldolase, 158 kDa; ovalbumin, 43 kDa; chymotrypsinogen A, 25 kDa; ribonuclease A, 13.7 kDa; aprotinin, 6.5 kDa) in the same buffer and at the same flow rate.

ESI-MS. Samples [50 μL of $KdpC_{sol}$ at 0.2 mg/mL in 50 mM sodium phosphate (pH 7.4) and 0.5 mM PMSF] were applied to a Vydac C4 HPLC column (4.6 mm × 25 mm) equilibrated with 95% water, 5% acetonitrile, and 0.03% TFA. Peptides were eluted with an increasing gradient of 80% acetonitrile, 20% water, and 0.03% TFA. One percent of the elutates was used directly for electrospray ionization (liquid chromatography-coupled MS). Detection of ions was carried out with an ion source mass spectrometer equipped with an ion trap (Esquire HCT, Bruker Daltonics) in the positive mode under the following conditions: dry temperature of 300 °C, capillary voltage of −4000 V, end plate offset of −500 V, skimmer of 40 V, and cap exit of 166 V. The determination of molecular weights and of protein sequence from corresponding MS/MS2 data sets was performed by deconvolution of the multiple charged peptide ions using Bruker Daltonics Esquire 5.2 DataAnalysis, version 3.2.

CD Spectroscopy. Spectra were collected on a Jasco J-810 spectropolarimeter equipped with a 0.1 mm path length quartz cell at room temperature, with the polarimeter calibrated by use of (+)-10-camphorsulfonic acid according to ref *16*. For each data set, 10 spectra were acquired at a scan speed of 50 nm/min with a step resolution of 1 nm together with a response time of 1 s and a bandwidth of 1 nm. Spectra were co-added and corrected with the corresponding buffer spectra collected the same way. To obtain a good signal-to-noise ratio, especially in the case of added nucleotides, samples were measured at a rather high protein concentration of 1 mg/mL in 50 mM sodium phosphate (pH 7.4) and 0.5 mM PMSF. ICD analysis was performed by the addition of increasing amounts of ATP dissolved in buffer directly to the cuvette followed by a 5 min incubation period prior to the measurements. Data sets were converted to mean residue ellipticity using a mean residue weight of 115 and deconvoluted by the self-consistent method with the SELCON algorithm (*17*). Computational analysis of protein structure was performed by use of the JNET secondary structure prediction algorithm (*18*).

8-Azido-ATP Labeling of $KdpC_{sol}$. Labeling of $KdpC_{sol}$ was performed in 50 μL aliquots at a protein concentration of 0.2 mg/mL in 50 mM sodium phosphate (pH 7.4) and 0.5 mM PMSF. 8-Azido-ATP (100 μM, MP Biomedicals) with $MgCl_2$ was added to the sample and the mixture incubated on ice for 10 min prior to irradiation. Photoinduced cross-linking of the probe was achieved with UV light (312 nm) by use of a 15 W hand-held UV lamp (HL-15-M, Bachofer) at a distance of 4 cm for 5 min on ice. In the case of nucleotide competition assays, $KdpC_{sol}$ was incubated with either ATP, ADP, AMP, GTP, or CTP together with $MgCl_2$ in equimolar concentrations of 5, 20, and 50 mM for 10 min on ice prior to the addition of the 8-azido-ATP. For trypsinolysis, 50 μL of $KdpC_{sol}$ at a protein concentration of 1 mg/mL was taken for the labeling procedure. Following irradiation, the sample was provided with 1 μg of trypsin (recombinant, proteomics grade, Roche catalog number 03708985001) and incubated at 20 °C for 14 h. All of the samples were subsequently subjected to ESI-MS analysis as described above.

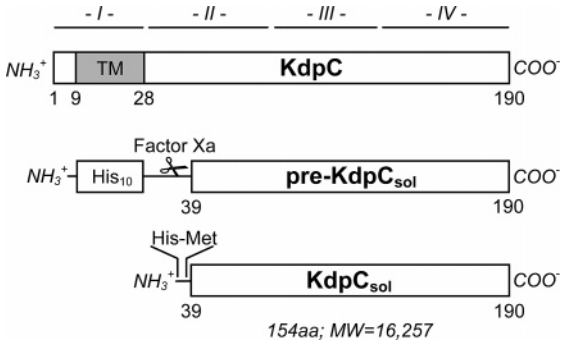

FIGURE 1: Construction scheme of $KdpC_{sol}$. Roman italics designate the four segments of the polypeptide according to ref *10*. Numbers indicate residues within the KdpC sequence. TM, transmembrane helix; His_{10}, polyhistidine affinity tag; Factor Xa, protease cleavage site.

Standard Procedures and Assays. Proteins were separated by SDS−PAGE using 16.5% T/6% C separating gels together with 4% T/3% C stacking gels (*19*) and stained with Coomassie Brilliant Blue G250. Whole cells were incubated for 5 min in sample application buffer prior to electrophoresis. Electroblotting was performed for 4 h at 0.6 A and 4 °C with 10 mM $NaHCO_3$, 3 mM Na_2CO_3, and 20% methanol as transfer buffer on either Protran nitrocellulose membranes (Whatman) for immuno-etection or Immobilon-P polyvinylidene difluoride (PVDF) membranes for N-terminal sequencing. Immunoblots were developed according to the method of ref *20* by use of the penta-His monoclonal antibody (Qiagen) at a dilution of 1:10000. N-Terminal sequencing of $KdpC_{sol}$ was performed via Edman degradation on an ABI 473 A pulsed liquid-phase protein sequencer (Applied Biosystems). Protein concentrations were assayed with the bicinchoninic acid (BCA) assay used as recommended by the supplier (Pierce) with bovine serum albumin as the standard.

RESULTS

Construction of KdpCsol. On the basis of protein topography analyses and sequence comparisons (*10*), KdpC has been divided into four segments (Figure 1), two of which (namely, segments II and IV) are highly conserved among bacterial species. Segment I contains the membrane-anchoring α-helix of the protein, whereas the C-terminal part (segment IV) is supposed to interact with KdpB. Especially segment IV has been demonstrated to be functionally important, since C-terminal deletions led to a nonfunctional phenotype (*10*). In addition, as already mentioned, KdpC has been shown to react with radioactive 2-azido-ATP within this stretch of residues (S. Dröse and K. Altendorf, unpublished results). To further elucidate a possible regulatory function of KdpC on enzyme activity and nucleotide interaction, the soluble part of the polypeptide ranging from residue Asn39 to Glu190 was expressed separately. This facilitates further

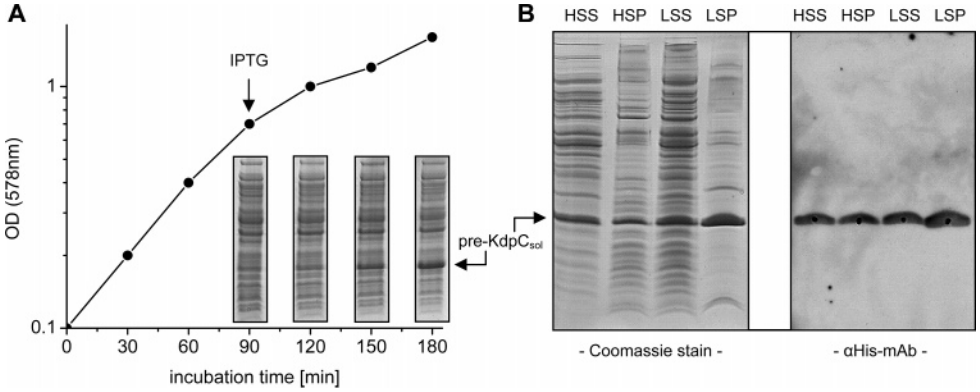

FIGURE 2: Synthesis of pre-KdpC$_{sol}$ and cell fractionation. (A) Growth curve of *E. coli* BL21/pET-kdpCsol and induction of protein synthesis. Cells were grown on rich medium, and gene expression was induced by the addition of 1 mM IPTG at an OD_{578} of 0.7. Insets demonstrate overexpression of pre-KdpC$_{sol}$ after induction (30 μg/lane of whole cells loaded on a SDS−PAGE gel). (B) Cell fractionation of induced BL21/pET-kdpCsol cells in Coomassie staining (left) and immunodetection (right). Ten micrograms of protein was applied per lane for SDS−PAGE. HSS, high-speed supernatant; HSP, high-speed pellet; LSS, low-speed supernatant; LSP, low-speed pellet.

analyses, especially by ESI-MS with respect to nucleotide binding and phosphorylation, without the use of detergent. To achieve high rates of protein synthesis, the corresponding part of the *kdpC* gene was cloned into a pET-16b vector, which enables IPTG-inducible gene expression. The resulting gene product, pre-KdpC$_{sol}$, comprises a His_{10} affinity tag, enabling affinity chromatography, followed by a factor Xa protease cleavage site to separate the His_{10} motif. Due to the vector background, the final cleavage product, KdpC$_{sol}$, features two additional amino acid residues (His and Met) preceding Asn39 of KdpC, which results in 154 amino acids with a calculated molecular weight of 16 257.

Protein Synthesis. Following induction of the growing *E. coli* BL21/pET-kdpCsol cells with IPTG, the growth rate exhibited a temporary decrease, which is characteristic for high rates of protein synthesis (Figure 2A). Concomitantly, the cells started to produce large amounts of pre-KdpC$_{sol}$, resulting in a final yield of approximately 10% of the whole cell protein as judged by densitometric comparison of the gel bands. To check whether this high rate of protein synthesis led to protein aggregation or to the formation of inclusion bodies, a cell fractionation via differential centrifugation was performed (Figure 2B). In subsequent SDS−PAGE, the identity of pre-KdpC$_{sol}$ was additionally proven by polyhistidine-specific immunoblotting. The vast majority of the polypeptide can be found in both the low-speed pellet and the high-speed pellet, thus already indicating a strong tendency to aggregate in the case of high concentrations. Nevertheless, large amounts of soluble pre-KdpC$_{sol}$ can be found in the high-speed supernatant, which was used for purification.

Isolation and Identification of KdpC$_{sol}$. Pre-KdpC$_{sol}$ was further purified from the high-speed supernatant fraction via Ni^{2+} affinity chromatography. Incubation of the supernatant with the affinity resin resulted in complete and specific immobilization of the protein, since almost no pre-KdpC$_{sol}$ was detectable in the elution steps with 10 and 55 mM imidazole (Figure 3). The shift to 170 mM imidazole led to a complete elution of pure protein with an expected apparent size of approximately 20 kDa. So that protein structure would not be biased during further analysis, the affinity tag was subsequently removed from pre-KdpC$_{sol}$ by factor Xa protease treatment with a rate of approximately 95%. Both uncleaved protein and separated His tag could be immobilized with a final additional Ni^{2+} affinity resin, with pure

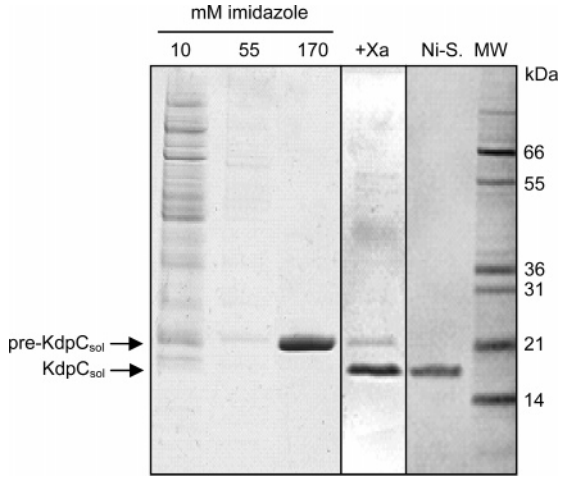

FIGURE 3: Isolation of KdpC$_{sol}$. Samples were loaded on a SDS−PAGE gel and stained with Coomassie Brilliant Blue. Elution steps (10 μL per lane) from Ni^{2+} affinity chromatography with 10, 55, and 170 mM imidazole: +Xa, purified pre-KdpC$_{sol}$ treated with factor Xa protease (3 μg/lane); Ni-S, isolated KdpC$_{sol}$ (2 μg/lane) after immobilization of the cleaved His tag and uncleaved pre-KdpC$_{sol}$ on Ni-Sepharose; MW, molecular weight standards (sizes indicated).

16 kDa KdpC$_{sol}$ cleavage product remaining in the flow-through. N-Terminal sequencing of the first 20 residues of KdpC$_{sol}$ revealed that protease treatment was uniform and specific, with the expected sequence (H-M-N-G-S-L-I-R-E-G-D-T-V-R-G-S-A-L-I-G).

Despite homogeneity, two protein peaks could be observed in the following nondenaturing size exclusion chromatography of KdpC$_{sol}$ (Figure 4). Size calibration of the column revealed that the second peak exactly corresponds to the expected size of KdpC$_{sol}$, whereas the first peak, which is much broader, represents a size corresponding to KdpC$_{sol}$ oligomers. When analyzed via denaturing SDS−PAGE, both peaks represent KdpC$_{sol}$ (data not shown). The two peaks in the gel filtration analysis were only observed at higher protein concentrations (>0.4 mg/mL). In the case of low concentrations of KdpC$_{sol}$, only the second peak corresponding to the monomer was observed (data not shown). Together with the tendency to form aggregates, which was already observed in the overexpression assay, this points toward an unspecific oligomerization of KdpC$_{sol}$ at high protein concentrations. Since the oligomerization status is crucial for further analysis,

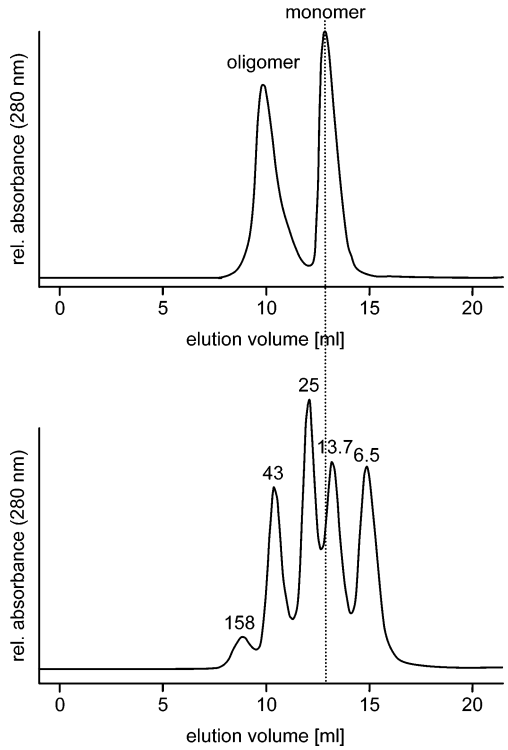

FIGURE 4: Size exclusion chromatography of isolated $KdpC_{sol}$. In the top panel is purified $KdpC_{sol}$ (5 mg/mL). The peaks corresponding to monomeric and oligomeric $KdpC_{sol}$ are indicated. In the bottom panel is the molecular weight calibration (standard protein sizes indicated). The dotted line indicates the position of monomeric $KdpC_{sol}$ with an expected molecular weight of 16 257.

the stability of the monomeric fraction was tested by concentrating and reapplying the monomer sample to gel filtration. The monomeric form of $KdpC_{sol}$ appeared to be stable, since only the monomer peak could be observed in the case of protein concentrations of up to 20 mg/mL suitable for NMR analysis (data not shown). Thus, only the monomeric fraction of the isolated $KdpC_{sol}$ was taken for further investigations.

To eventually test the integrity of the isolated $KdpC_{sol}$ with respect to potential modifications, the polypeptide was taken for denaturing ESI-MS analysis. Since the mass spectrometer was coupled to liquid chromatography (hydrophobic interaction HPLC), the resulting HPLC/ESI-MS profiles provide information about both the biochemical properties and the molecular mass of the peptides analyzed. The HPLC chromatogram again showed just one protein peak without any contaminating signals (Figure 5). Accordingly, only a single mass peak was observed simultaneously in the ESI-MS analysis. The molecular weight determined from the peptide ion pattern was 16 257, which exactly matches the expected molecular weight as calculated from the primary sequence. Thus, the isolated $KdpC_{sol}$ contains no further modifications.

Secondary Structure Analysis. Structural properties of $KdpC_{sol}$ were investigated with CD spectroscopy [Figure 6 (●)]. The isolated polypeptide exhibited a highly α-helical ellipticity spectrum, with a characteristic maximum at 190 nm combined with two minima at 207 and 221 nm and the isoelliptic point at 198 nm. The spectrum was subsequently deconvoluted to consist of 44% α-helices together with 8% β-sheet conformation. Since the predicted secondary structure calculated from the primary sequence comprises 39% α-helices and 7% β-sheets, these data strongly indicate that the isolated $KdpC_{sol}$ adopts its native conformation.

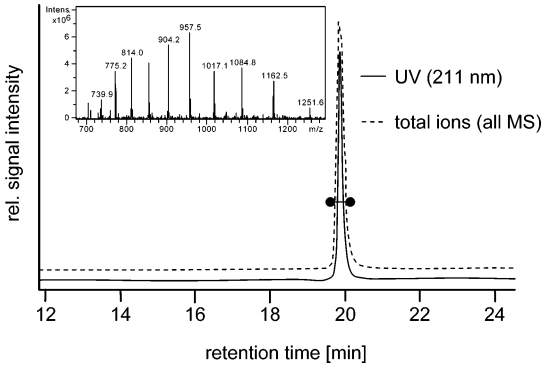

FIGURE 5: Liquid chromatography-coupled ESI-MS profile of $KdpC_{sol}$. Isolated $KdpC_{sol}$ (0.2 mg/mL) was subjected to HPLC separation with the eluates directly subjected to ESI-MS analysis. Both the HPLC elution profile (measured at 211 nm) and the total ion chromatogram of the mass spectrometer are presented. Molecular mass calculation was performed from ions eluted with retention times between 19.7 and 20.1 min (as indicated by the dumbbell), resulting in a molecular weight of 16 257. The corresponding mass spectrum is depicted in the inset.

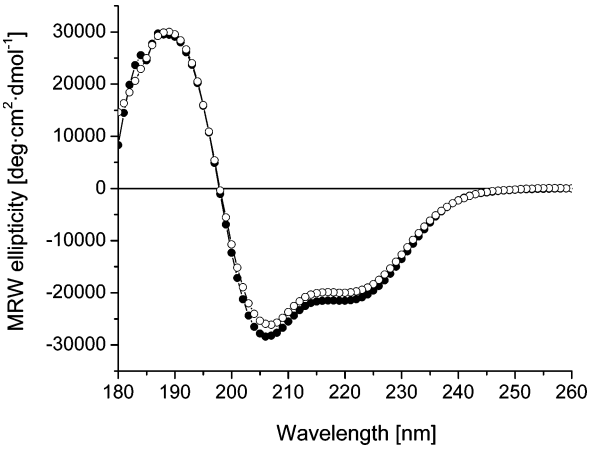

FIGURE 6: Circular dichroism spectroscopy of $KdpC_{sol}$. Isolated $KdpC_{sol}$ was measured at a concentration of 1 mg/mL in 50 mM sodium phosphate (pH 7.4) and 0.5 mM PMSF (●). For ICD analysis, 2 mM ATP was added to the cuvette (○). Spectra were converted to mean residue weight (MRW) ellipticity assuming a mean residue weight of 115.

To elucidate whether an additional regulatory high-affinty ATP binding site exists within the protein, $KdpC_{sol}$ was also investigated via ICD spectroscopy. When a ligand binds to a peptide or protein, it acquires an induced CD spectrum by chiral pertubation or electron rearrangements (*21*). The intensity of the resulting ICD spectrum is, thus, proportional to the affinity and geometry of ligand interaction. $KdpC_{sol}$ was, therefore, titrated with increasing amounts of nucleotide directly in the cuvette, resulting in ATP concentrations of 10, 100, 500, 1000, and 2000 μM. None of the resulting ICD spectra showed significant changes with respect to the control without added nucleotide. The spectral characteristics (i.e., the position of the maximum and the two minima) as well as the amplitude and the isoelliptic point were identical in every case. The small differences, which were obtained only at the high concentration of 2 mM ATP [Figure 6 (○)], are most likely more due to the increasing spectroscopic disturbance of the nucleotide itself rather than to alterations in protein structure. Although all spectra were corrected for

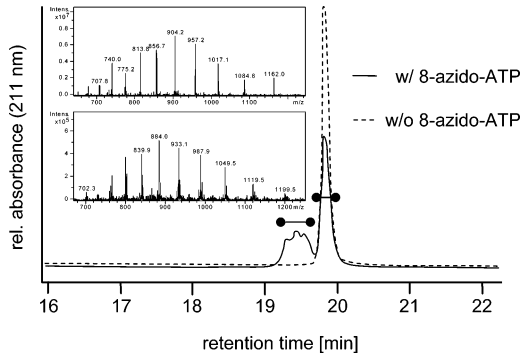

FIGURE 7: Liquid chromatography-coupled ESI-MS analysis of 8-azido-ATP-labeled $KdpC_{sol}$. Isolated $KdpC_{sol}$ (0.2 mg/mL) was labeled with 100 μM 8-azido-ATP and analyzed by HPLC-coupled ESI-MS. The HPLC elution profiles (measured at 211 nm) of both labeled (—) and unlabeled $KdpC_{sol}$ (- - -) are presented. Molecular weight calculations were performed from ions eluted between the indicated retention times (depicted by the dumbbells), resulting in values of 16 777 and 16 257, respectively. The corresponding mass spectra are shown as insets, with the spectrum for unlabeled $KdpC_{sol}$ on top.

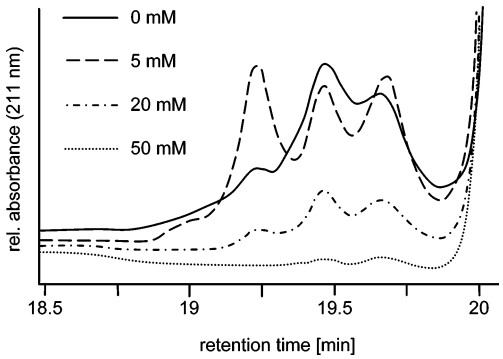

FIGURE 8: ATP quenching of 8-azido-ATP labeling of $KdpC_{sol}$. Isolated $KdpC_{sol}$ (0.2 mg/mL) was preincubated with increasing amounts of ATP (5, 20, and 50 mM) prior to the addition of 8-azido-ATP (100 μM) and photoactivation. Samples were then analyzed by HPLC-coupled ESI-MS. Only the UV chromatogram corresponding to the 8-azido-ATP-labeled fraction of $KdpC_{sol}$ is presented for clarity. ATP concentrations are given.

the presence of nucleotide by subtraction of the corresponding buffer/ligand spectra, the strong chirality of the ligand covers the signals of interest at high ATP concentrations. Thus, a high-affinity ATP binding site within $KdpC_{sol}$ could not be detected.

Labeling of $KdpC_{sol}$ with 8-Azido-ATP. ICD spectroscopy revealed that there was no binding of ATP to $KdpC_{sol}$ with high affinity. However, since the peptide represents only the soluble portion of KdpC, which is normally supposed to interact with KdpB, an increase in binding affinity might occur in the case of protein interaction. As a prerequisite, there should be a defined low-affinity nucleotide binding site in $KdpC_{sol}$. In previous work, it was shown that KdpC can be labeled with radioactive [^{32}P]-2-azido-ATP within the assembled KdpFABC complex. These experiments did not further elucidate whether azido-ATP binding occurred specifically to a defined binding site within the protein or if KdpC just caught an ATP molecule from the neighboring catalytic nucleotide binding domain of KdpB. Thus, $KdpC_{sol}$ was treated with the nonradioactive photoactivatable 8-azido-ATP to trap the nucleotide also within a potential low-affinity binding site and to analyze the labeling specificity with ESI-MS. The free acid of 8-azido-ATP has a molecular weight of 548. During the photoreaction, N_2 is released due to the formation of the reactive nitrene, resulting in a molecular weight of 520 for the bound ATP analogue. Thus, a corresponding increase in molecular weight should be detectable with mass spectrometry.

$KdpC_{sol}$ was reacted with 100 μM 8-azido-ATP and subsequently subjected to liquid chromatography-coupled ESI-MS (Figure 7). In the resulting chromatogram, two peaks could be detected, one of which represents the unlabeled polypeptide together with an additional tripartite protein peak representing the labeled fraction of $KdpC_{sol}$. A labeling ratio of ~45% was calculated by integration of the two peaks. Deconvolution of the corresponding mass spectra resulted again in a molecular weight of 16 257 for the unlabeled $KdpC_{sol}$, thereby indicating that no damage occurred to the protein by the UV irradiation. Surprisingly, there was only one mass spectrum that could be detected within the tripartite peak, corresponding to a molecular weight of 16 777, which exactly matches the expected value if just one molecule of 8-azido-ATP is bound to $KdpC_{sol}$. Thus, the tripartite shape of the protein peak does not resemble that of multiple-nucleotide incorporation but just one molecule of 8-azido-ATP possibly bound to different sites within the peptide, thereby slightly altering its elution properties determined via HPLC. Accordingly, mass spectra representing the incorporation of two or more molecules of 8-azido-ATP could not be detected anywhere in the data set. Together with the high labeling efficiency of almost 50%, this already strongly supported the notion that the labeling was specific, since in the case of unspecific binding of the nucleotide at least doubly labeled $KdpC_{sol}$ should have occurred with a probability of 20−25%. Incorporation of two molecules of 8-azido-ATP could only be observed at a rate of merely 10% with respect to the single labeled fraction when the nucleotide was used at high concentrations of 1 mM in the photoreaction (data not shown). Furthermore, 8-azido-ATP labeling was completely abolished in the presence of 0.2% SDS in the samples. The corresponding ESI-MS analysis only revealed the molecular weight of the unlabeled $KdpC_{sol}$ together with a proper well-defined peak in the UV chromatogram (data not shown). Taken together, these experiments clearly indicate the presence of a structurally well-defined nucleotide binding site within $KdpC_{sol}$.

To test for nucleotide specificity in the ATP binding of $KdpC_{sol}$, 8-azido-ATP competed with different nucleotides at varying concentrations. First, the protein was preincubated with increasing amounts of ATP (5, 20, and 50 mM) prior to the addition of the photoactivatable nucleotide, which is in the range known to prevent the labeling with 8-azido-ATP (*22*) (Figure 8). The preincubation with 5 mM ATP had no competing effect on the binding of 8-azido-ATP, whereas the tripartite shape of the peak was slightly shifted with respect to the amplitude of the single components. Again, also the fine evaluation of the corresponding mass spectra of each component revealed only one proper molecular weight of 16 777, resembling one molecule of 8-azido-ATP bound to $KdpC_{sol}$. Thus, in the presence of 5 mM ATP, the nucleotide binding is only slightly influenced but not abolished. In contrast, the presence of 20 and 50 mM ATP led to a quench of ~75 and ~98%, respectively, in the labeling efficiency. The shape of the corresponding chromatograms again resembled that of the noncompeted sample,

thereby indicating that now the binding is completely blocked. These shifts in the tripartite peak pattern again indicate that there is only one nucleotide binding site, which is gradually affected by the competing ATP. Furthermore, even in the presence of 50 mM ATP, no phosphorylation product of $KdpC_{sol}$ could be observed with ESI-MS, thereby excluding any possible regulatory mechanism involving autophosphorylation.

Surprisingly, a set of experiments with 5, 20, and 50 mM ADP, AMP, GTP, and CTP resulted in the same quenching rates of the 8-azido-ATP labeling (data not shown), thus revealing an apparantly low specificity for the nucleotide. However, the shifts in the peak pattern in the presence of 5 mM competing nucleotide were significantly different, with ADP and AMP more promoting the formation of the first component at the expense of the second. In contrast, this first component was completely absent in the case of 5 mM GTP. Thus, although there is a rather low overall nucleotide specificity of $KdpC_{sol}$, the differential competition pattern in the presence of 5 mM competing nucleotide suggests discriminative preferences of 8-azido-ATP for different sites of cross-linking within the binding site under conditions of weak competition.

Location of the 8-Azido-ATP Binding Site within $KdpC_{sol}$. To finally confirm the presence of just one specific binding site for ATP within $KdpC_{sol}$, the protein was digested with trypsin and subsequently analyzed by ESI-MS. Tryptic digestion resulted in complete peptide fragmentation as judged by the preceding MS-coupled HPLC run (data not shown). With the exception of a single six-residue fragment at the N-terminus of $KdpC_{sol}$ (Glu45−Arg50, KdpC nomenclature), all of the fragments could be recovered and identified in the corresponding MS/MS2 data sets. Thus, unlabeled and 8-azido-ATP-labeled $KdpC_{sol}$ were taken for comparative analysis. The mass spectra of the labeled sample revealed only one cleavage product with an increase in the monoisotopic molecular weight corresponding to a bound 8-azido-ATP, namely, from 1981.16 for unlabeled $KdpC_{sol}$ to 2501.95 in the sample taken for the ATP labeling, which exactly matches the expected increment of 520. No other labeling products could be detected throughout the whole data set, although the labeling rate was again nearly 50%. By its molecular weight (MS data) and by simultaneous MS2 sequence analysis, the corresponding peptide was clearly identified as the Val144−Lys161 fragment. Thus, the binding of ATP could be demonstrated to occur at a well-defined binding site, although the tripartite shape of the corresponding HPLC profile supports the notion that the 8-azido-ATP could be cross-linked to different sites within this stretch of residues.

DISCUSSION

P-Type ATPases usually consist of a single catalytic subunit, which is responsible for both substrate transport and ATP hydrolysis. There are several examples of additional regulatory subunits affecting protein activity like phospholamban and calmodulin in the case of the Ca^{2+}-ATPase or the γ-subunit of Na^+,K^+-ATPase. Regulatory function is exerted either via steric interactions with the dynamically moving catalytic domains (*14*) or by directly affecting the affinity of the nucleotide binding site for ATP (*13*). All of these additional subunits consist of a single transmembrane span, which anchors the polypeptide in the membrane, together with a cytoplasmic extension with regulatory properties.

The KdpFABC complex resembles a unique form of P-type ATPases, since catalytic activity and sites of substrate transport are located on different subunits. However, by comparative structural analysis of the nucleotide binding domain of the ATP-hydrolyzing KdpB subunit, the overall catalytical features of P-type ATPases are also present within the KdpFABC complex (*23*). Among the four subunits of the complex, KdpC also comprises a single transmembrane span together with a rather long hydrophilic domain, which is oriented toward the cytoplasm. Although the protein has not yet been characterized extensively, it was shown that it is absolutely essential for the activity of the transport complex (*10*). Especially the highly conserved C-terminal portion of the polypeptide was found to be important, since deletion mutagenesis revealed that the truncation of 11 residues led to the inactivation of the complex (*10*). Furthermore, KdpC was shown to significantly react with the radioactive probe [^{32}P]-2-azido-ATP, thereby suggesting at least nucleotide interaction if not binding. However, it was not shown whether the radiolabel was incorporated due to specific interactions or in just a passive, unspecific manner due to its spatial proximity to the catalytic domain of the complex. Here, we clearly demonstrate that $KdpC_{sol}$ does bind ATP, although with a rather low affinity and specificity, and that nucleotide binding occurs specifically within a structurally well defined binding site within the polypeptide.

Two putative mechanisms of regulation existing in other P-type ATPases could be excluded in this study. First, a possible (auto)phosphorylation could not be observed in the ESI-MS analysis even in the presence of 50 mM ATP. Second, a putative inhibitory function seems rather unlikely, since the presence of even a 10-fold excess of isolated $KdpC_{sol}$ did not affect the rates of ATP hydrolysis of the KdpFABC complex (data not shown). For the *N. crassa* plasma membrane H^+-ATPase, similar experiments revealed an inhibitory function of the intrinsic regulatory domain, if a corresponding synthetic peptide was co-added to a standard ATPase assay (*14*). Thus, KdpC most likely exerts an activating effect, which cannot be observed in a corresponding experiment with $KdpC_{sol}$ together with completely assembled KdpFABC complexes, which already comprise the full-length KdpC subunit. An activating function is further supported by the above-mentioned truncation analysis, which resulted in inactive transport complexes if the C-terminal region of KdpC is affected. Nevertheless, an ATP-dependent regulatory function cannot merely be attributed to interactions with the nucleotide, since the affinity of $KdpC_{sol}$ is rather low. In ICD spectroscopy, the ATP binding site could not be titrated with ATP concentrations of up to 2 mM, which is in accord with the 8-azido-ATP competition assay, in which a quench of the photoactivatable probe occurred only in the presence of 20 and 50 mM ATP, which is far from the physiological concentration of 3 mM ATP in the cytoplasm. However, the peak shift pattern in the competition also revealed that there is a fine-tuning of nucleotide binding with multiple possible reaction sites for the activated nitrene within the binding site, which are variably preferred depending on the competing nucleotide. However, both the low

nucleotide affinity and specificity render a cooperative regulatory mechanism likely. The site of ATP binding could be located within conserved C-terminal segment IV of KdpC. This stretch of residues can easily come into contact with the catalytic domains of the KdpB subunit. Such an interaction could already be abolished by C-terminal truncations of the peptide. Thus, the formation of a ternary complex of the hydrophilic domain of KdpC together with KdpBN (the nucleotide binding domain of KdpB) and the nucleotide is, although speculative, quite reasonable for the following reasons. Isolated KdpBN has a rather high binding constant for ATP of 1.4 mM (*23*). In contrast, the other well-characterized nucleotide binding domains feature a much better K_d for ATP, i.e., 10−100 μM in the case of the Ca^{2+}-ATPase (*24*) or 70 μM for the Wilson disease protein, which is reported to be within the typical range of simple protein/ligand systems (*25*). Another special feature of KdpBN with respect to Wilson disease protein is that in the former there are no interactions between the ribose moiety of the nucleotide and the protein (*23*) whereas in the latter the ribose is well coordinated within a proper ribose binding pocket (*25*), which might explain the low ATP affinity of KdpBN. Furthermore, in KdpBN, the nucleotide has to be oriented to enter the binding site properly together with a precisely balanced equilibrium of nucleotide uptake and release (*23*). Together with the low nucleotide affinity and the lack of additional coordination sites targeting the ribose moiety, this renders an additional regulatory process likely. At least in the case of Wilson disease protein, there is no additional subunit or regulatory domain. Although phospholamban or calmodulin is present in the Ca^{2+}-ATPase as already mentioned, the mode of regulation most likely differs from that of KdpFABC due to an evolutionary early divergence of mammalian and bacterial P-type ion pumps. Since the Wilson disease protein is more closely related to KdpB than to the Ca^{2+}-ATPase, these two mechanisms of nucleotide interactions can be directly compared (*25*). Interestingly, in our experiments, neither the phosphate moiety (i.e., the comparison of ATP, ADP, and AMP) nor the base (ATP vs GTP and CTP) of the competing nucleotide had any influence on the overall 8-azido-ATP labeling ratio. In addition, within the 8-azido-ATP, the reactive nitrene is located right next to the ribose, which altogether argues in favor of a rather untypical interaction between $KdpC_{sol}$ and ATP via the ribose moiety of the nucleotide, although there is yet no direct experimental evidence for such an interaction. However, this view is further supported by sequence analysis of the ATP-binding stretch of residues in $KdpC_{sol}$, in which no typical consensus motif could be found. This ribose-mediated interaction would also explain the rather low nucleotide affinity with respect to a well-coordinated high-affinity binding, which involves both the base and the phosphates. Taken together, the soluble part of KdpC might aid the nucleotide via ribose interaction to enter the low-affinity catalytic binding site in KdpBN. This view of an essential role of KdpC during catalysis is further strongly supported by the fact that isolated KdpB exhibits no hydrolytic activity. Activity could, however, not be restored by the addition of $KdpC_{sol}$ (data not shown), which is most likely due to the lack of the membrane part, which orients the proteins in a proper way.

An interaction of $KdpC_{sol}$ with KdpBN around the catalytic nucleotide binding site has most recently been demonstrated doubtlessly by NMR analysis (to be published elsewhere). However, the exact mechanism of this novel regulatory feature within the KdpFABC complex must be further elucidated by, for example, mutagenesis of the putative ribose binding motif or NMR analysis of the solution structure of $KdpC_{sol}$, which is under way in our laboratory.

ACKNOWLEDGMENT

We thank Stefan Walter (Angewandte Genetik der Mikroorganismen, Universität Osnabrück) for his generous help with the ESI-MS. Monika Nitschke is kindly acknowledged for technical assistance in the cloning of plasmid pET-kdpCsol.

REFERENCES

1. Møller, J. V., Juul, B., and le Maire, M. (1996) Structural organization, ion transport, and energy transduction of P-type ATPases, *Biochim. Biophys. Acta 1286*, 1−51.
2. Toyoshima, C., Nakasako, M., Nomura, H., and Ogawa, H. (2000) Crystal structure of the calcium pump of sarcoplasmic reticulum at 2.6 Å resolution, *Nature 405*, 647−655.
3. Toyoshima, C., and Mizutani, T. (2004) Crystal structure of the calcium pump with a bound ATP analogue, *Nature 430*, 529−535.
4. Young, H. S., and Stokes, D. L. (2004) The mechanics of calcium transport, *J. Membr. Biol. 198*, 55−63.
5. Altendorf, K., Ga*β*el, M., Puppe, W., Möllenkamp, T., Zeek, A., Boddien, C., Fendler, K., Bamberg, E., and Dröse, S. (1998) Structure and function of the Kdp-ATPase of *Escherichia coli*, *Acta Physiol. Scand. Suppl. 643*, 173−146.
6. Van der Laan, M., Ga*β*el, M., and Altendorf, K. (2002) Characterization of amino acid substitutions in KdpA, the K^+-binding and -translocating subunit of the KdpFABC complex of *Escherichia coli*, *J. Bacteriol. 184*, 5491−5494.
7. Durell, S. R., Bakker, E. P., and Guy, H. R. (2000) Does the KdpA subunit from the high affinity K^+-translocating P-type KDP-ATPase have a structure similar to that of K^+ channels? *Biophys. J. 77*, 775−788.
8. Bramkamp, M., and Altendorf, K. (2005) Single amino acid substitution in the putative transmembrane helix V in KdpB of the KdpFABC complex of *Escherichia coli* uncouples ATPase activity and ion transport, *Biochemistry 44*, 8260−8266.
9. Ga*β*el, M., Möllenkamp, T., Puppe, W., and Altendorf, K. (1999) The KdpF subunit is part of the K^+-translocating Kdp complex of *Escherichia coli* and is responsible for stabilization of the complex in vitro, *J. Biol. Chem. 274*, 37901−37907.
10. Ga*β*el, M., and Altendorf, K. (2001) Analysis of KdpC of the K^+-transporting KdpFABC complex of *Escherichia coli*, *Eur. J. Biochem. 268*, 1772−1781.
11. Axelsen, M. G., and Palmgren, K. B. (1998) Evolution of substrate specificities in the P-type ATPase superfamily, *J. Mol. Evol. 46*, 84−101.
12. Kimura, Y., and Inui, M. (2002) Reconstitution of the cytoplasmic interaction between phospholamban and Ca^{2+}-ATPase of cardiac sarcoplasmic reticulum, *Mol. Pharmacol. 61*, 667−673.
13. Therien, A. G., Karlish, S. J. D., and Blostein, R. (1999) Expression and functional role of the γ subunit of the Na, K-ATPase in mammalian cells, *J. Biol. Chem. 274*, 12252−12256.
14. Kühlbrandt, W., Zeelen, J., and Dietrich, J. (2002) Structure, mechanism, and regulation of the *Neurospora* plasma membrane H^+-ATPase, *Science 297*, 1692−1696.
15. Sambrook, J., Fritsch, E. F., and Maniatis, T. (1989) *Molecular Cloning. A Laboratory Manual*, Cold Spring Harbor Laboratory Press, Plainview, NY.
16. Johnson, W. C., Jr. (1988) Secondary structure of proteins through circular dichroism spectroscopy, *Annu. Rev. Biophys. Biophys. Chem. 17*, 145−166.
17. Sreerama, N., and Woody, R. W. (1994) Protein secondary structure from circular dichroism spectroscopy. Combining vari-

able selection principle and cluster analysis with neural network, ridge regression and self-consistent methods, *J. Mol. Biol. 242*, 497−507.
18. Cuff, J. A., and Barton, G. J. (2000) Application of enhanced multiple sequence alignment profiles to improve protein secondary structure prediction, *Proteins: Struct., Funct., Genet. 40*, 502−511.
19. Schägger, H., and von Jagow, G. (1987) Tricine-sodium dodecyl sulfate-polyacrylamide gel electrophoresis for the separation of proteins in the range of 1 to 100 kDa, *Anal. Biochem. 166*, 368−379.
20. Birkenhäger, R., Greie, J.-C., Altendorf, K., and Deckers-Hebestreit, G. (1999) F_O complex of the *Escherichia coli* ATP synthase, *Eur. J. Biochem. 264*, 385−396.
21. Rodger, A., Marrington, R., Roper, D., and Windsor, S. (2005) Circular dichroism spectroscopy for the study of protein-ligand interactions, *Methods Mol. Biol. 305*, 343−364.
22. Heermann, R., Altendorf, K., and Jung, K. (2000) The hydrophilic N-terminal domain complements the membrane-anchored C-terminal domain of the sensor kinase KdpD of *Escherichia coli*, *J. Biol. Chem. 275*, 17080−17085.
23. Haupt, M., Bramkamp, M., Heller, M., Coles, M., Deckers-Hebestreit, G., Herkenhoff-Hesselmann, B., Altendorf, K., and Kessler, H. (2006) The holo-form of the nucleotide binding domain of the KdpFABC complex from *Escherichia coli* reveals a new binding mode, *J. Biol. Chem. 281*, 9641−9649.
24. Abu-Abed, M., Mal, T. K., Kainosho, M., MacLennan, D. H., and Ikura, M. (2002) Characterization of the ATP-binding domain of the sarco(endo)plasmic reticulum Ca^{2+}-ATPase: Probing nucleotide binding by multidimensional NMR, *Biochemistry 41*, 1156−1164.
25. Dmitriev, O., Tsivkovskii, R., Abildgaard, F., Morgan, C. T., Markley, J. L., and Lutsenko, S. (2006) Solution structure of the N-domain of Wilson disease protein: Distinct nucleotide-binding environment and effects of disease mutations, *Proc. Natl. Acad. Sci. U.S.A. 103*, 5302−5307.

BI061213P